

A Novel Hamiltonian Replica Exchange MD Protocol to Enhance Protein Conformational Space Sampling

Roman Affentranger,[†] Ivano Tavernelli,[‡] and Ernesto E. Di Iorio^{*,†}

*Institut für Biochemie, Eidgenössische Technische Hochschule ETH-Zurich,
Schafmattstrasse 18, 8093 Zurich, Switzerland, and Institut de Chimie Moléculaire et
Biologique, BCH-LCBC, Ecole Polytechnique Fédérale de Lausanne,
1015 Lausanne, Switzerland*

Received October 13, 2005

Abstract: Limited searching in the conformational space is one of the major obstacles for investigating protein dynamics by numerical approaches. For this reason, classical all-atom molecular dynamics (MD) simulations of proteins tend to be confined to local energy minima, particularly when the bulk solvent is treated explicitly. To overcome this problem, we have developed a novel replica exchange protocol that uses modified force-field parameters to treat interparticle nonbonded potentials within the protein and between protein and solvent atoms, leaving unperturbed those relative to solvent–solvent interactions. We have tested the new protocol on the 18-residue-long tip of the P domain of calreticulin in an explicit solvent. With only eight replicas, we have been able to considerably enhance the conformational space sampled during a 100 ns simulation, compared to as many parallel classical molecular dynamics simulations of the same length or to a single one lasting 450 ns. A direct comparison between the various simulations has been possible thanks to the implementation of the weighted histogram analysis method, by which conformations simulated with modified force-field parameters can be assigned different weights. Interatom, inter-residue distances in the structural ensembles obtained with our novel replica exchange approach and by classical MD simulations compare equally well with those derived from NMR data. Rare events, such as unfolding and refolding, occur with reasonable statistical frequency. Visiting of conformations characterized by very small Boltzmann weights is also possible. Despite their low probability, such regions of the conformational space may play an important role in the search for local potential-energy minima and in dynamically controlled functions.

1. Introduction

Proteins are complex systems characterized by very rough free-energy landscapes (FEL). A feature that certainly contributes to complexity is the presence of anisotropic interactions—both within the protein and between the macromolecule and the surrounding solvent—where the coexistence of repulsive and attractive terms leads to many

degenerate local energy minima. Such minima are separated by free-energy barriers, whose heights are often much larger than the thermal energy available to the system. For this reason, conventional all-atom molecular dynamics (MD) simulations of proteins in explicit solvent at room temperature suffer of a problem known as kinetic trapping; namely, the system tends to remain confined within one of the many local energy minima. Therefore, physical quantities that depend on an extensive sampling of the conformational space cannot be adequately calculated. Furthermore, conformations with very small Boltzmann weights, which are likely to be

* Corresponding author tel.: +41-44-6323137; fax: +41-44-6321298; e-mail: diiorio@bc.biol.ethz.ch.

[†] Eidgenössische Technische Hochschule ETH–Hönggerberg.

[‡] Ecole Polytechnique Fédérale de Lausanne.

involved in processes of high biological relevance, such as conformational transitions and dynamically controlled functional events,¹ are not visited.

A possible remedy to this problem is to perform MD simulations in a generalized ensemble (for a review, see ref 2). The idea is to achieve a random walk in potential-energy space, which allows the system to easily overcome the energy barriers that separate local minima and, therefore, to sample a much wider phase space compared to conventional simulations. Three well-known approaches for carrying out generalized ensemble MD simulations are the multicanonical algorithm,^{3,4} simulated tempering,^{5,6} and the replica exchange method (REM).^{2,7–15} The former two algorithms make use of non-Boltzmann probability weight factors, which are not known a priori and need to be determined by trial simulations. This process is highly nontrivial and can be very tedious for complex systems such as proteins. In contrast, REM uses standard Boltzmann weight factors that are known a priori. A number of noninteracting simulations of the same system are performed in parallel, but under different conditions; at given time intervals, the simulation conditions are exchanged with a specific transition probability between replica pairs. Therefore, REM is particularly well-suited for parallel computing on simple PC clusters because it requires very little communication between the individual processors. The algorithm was originally developed for Monte Carlo simulations¹⁵ and has been adapted to MD simulations by Sugita and Okamoto.⁷ In its original implementation, the condition to be varied and exchanged among the replicas is the temperature. This results in a random walk in temperature space, which in turn induces a random walk in potential-energy space. Thus, systems that—when simulated by conventional methods at room temperature—would remain trapped within a limited region of the conformational space are allowed to escape more easily from local minima by jumping back and forth between high and low temperatures.

For large systems, such as proteins in an explicit solvent, temperature replica exchange MD (T-REMD) simulations have one major drawback: since the number of replicas needed to cover a given temperature range is roughly proportional to the square root of the number of degrees of freedom of the system,¹⁶ many replicas need to be simulated, thus, rendering T-REMD simulations of proteins in an explicit solvent very demanding in computational terms. Because efficient sampling requires diffusion in temperature space, the higher the number of replicas that are used, the longer the simulation has to be performed, or the more frequently exchanges have to be attempted. This limits the capability of the method to obtain—with equivalent computational effort—better thermodynamic sampling, compared to classical MD (CMD) simulations. A remedy to this shortcoming of T-REMD is given by the Hamiltonian REM,^{9,16,17} where the various replicas are simulated at constant or variable temperatures, but with different parameter sets for the equations of motion. This approach rests on the consideration that, since the individual simulations are independent and noninteracting, they need not necessarily be simulated using the same Hamiltonian. By restricting the changes introduced in the different Hamiltonians to only a

subset of the degrees of freedom of the system, the number of replicas needed to cover a given range in “effective temperature” can be greatly reduced compared to T-REMD simulations. Both standard T-REMD and Hamiltonian REMD (H-REMD) at constant temperature are, thus, one-dimensional formulations of the general REMD methodology.⁹ An obvious advantage of H-REMD at constant temperature is that no velocity rescaling⁷ is needed when exchanges between replicas take place. Additional details on replica exchange approaches are summarized in a recent review by Snow et al.¹⁸

There is evidence that the dynamic properties of a protein are influenced by the frustration of its interparticle nonbonded interactions.^{19–21} Therefore, H-REMD simulations, using modified force-field parameters for such interactions, are expected to enhance the sampling of the conformational space by directly influencing the frustration of the system and, therefore, its dynamic properties.

We report here the implementation of a new H-REMD protocol based on the simultaneous modification of electrostatic and Lennard-Jones (LJ) parameters, aiming also at testing this working hypothesis. Although not widespread in combination with H-REMD, the idea of modifying the force-field parameters used for classical MD simulations has already been exploited for locating the global minimum of the complex potential-energy hypersurface of oligopeptides.^{22,23} Subsequently, this approach has been further developed to simulate, for instance, protein folding²⁴ or to predict transmembrane helix packing.²⁵ We have used our H-REMD to simulate—in an explicit solvent—the 18-residue-long tip of the P domain of calreticulin, a chaperon involved in protein quality control in the endoplasmic reticulum.²⁶ Recently, the structure of the long, flexible, hairpin-like P domain of calreticulin was solved by NMR, along with those of increasingly smaller fragments of its tip. All the fragments are shown to adopt the same structure they do in the full-length hairpin.^{27–29} Now, also, the 18-residue-long polypeptide corresponding to the very tip of the calreticulin P domain has been investigated, but the data leave room for interpretation concerning its proteinlike folding behavior (L. Ellgaard, Institute of Biochemistry, ETH-Zurich, personal communication). Therefore, we used CRT18 as a test molecule for our new H-REMD protocol with the hope of gaining new insights on its folding properties.

2. Methods and Analysis

2.1. Simulation Details. All simulations were performed with the software package GROMACS 3.1.4,^{30,31} using the GROMOS 43a1 force field³² and periodic boundary conditions. Temperature (T) and pressure (P) were held constant using the weak coupling method,³³ with relaxation times of 0.1 ps for T and 0.5 ps for P . The protein and solvent, including ions, were each coupled separately to a temperature bath. All simulations were performed at 278 K under a pressure of 1 bar. An integration step of 2 fs was used, keeping bond lengths constant using the LINCS³⁴ algorithm for the peptide and SETTLE³⁵ for the water molecules. Nonbonded interactions were treated with the twin-range method, with cutoff radii of 0.8 and 1.4 nm, updating the

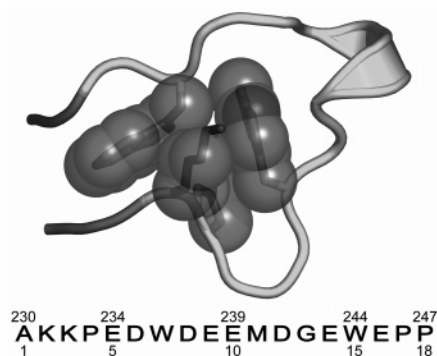


Figure 1. Structure of CRT18, as obtained from the coordinates of the larger 36 amino acid fragment (PDB entry 1K91), along with its amino acid sequence with the numbering pertaining to the full P domain of calreticulin (above the sequence), and that used in this work. This structure has been used as the starting configuration for all of our simulations and as reference for the analysis of the trajectories. The model highlights various regions of the molecule. Thus, the backbone is shown as a tube, with the first and last residues in dark gray; the side chains of the amino acids involved in the formation of the hydrophobic core as sticks, with the individual atoms that make up the core represented as transparent spheres; and the single α -helical turn, formed by residues 9–12, as a ribbon. This region is recognized by DSSP⁴⁶ as being α -helical in only 2 of the 20 structures deposited in the PDB file 1K91. The model was drawn using PYMOL (<http://www.pymol.org>).

pair lists every step or every five steps respectively for the short and long cutoff. Long-range electrostatic interactions were treated with the reaction-field approach,³⁶ using a cutoff radius of 1.4 nm and a dielectric constant for the reaction field of 68.³⁷

Initial coordinates for the 18-residue tip of the calreticulin P domain (see Figure 1) were obtained from the larger, 36 amino acid fragment (PDB entry 1K91²⁷). The system was solvated in an octahedral box with 2808 SPC/E³⁸ water molecules, leaving an initial minimum distance between the peptide and the box walls of 1.1 nm. Aliphatic hydrogen atoms were treated by the united-atoms approach. Acidic residues were assumed to be in the charged state corresponding to neutral pH, leading to a net charge of -6 . After energy minimization, the system was neutralized by adding eight sodium and two chlorine ions using the GROMACS program GENION. Following energy minimization of the neutralized system, the atoms were assigned random velocities drawn from a Maxwell distribution corresponding to 213 K. The system was then gradually heated to 278 K within 100 ps, applying a decreasing positional restraint to the protein atoms with force constants ranging between 25 000 and 0 kJ mol⁻¹ nm⁻². From this state, a 450-ns CMD simulation was performed (long CMD, LCMD) on a dual processor Pentium III (1266 MHz) computer. In addition, eight independent, 100-ns-long, CMD simulations (8CMD) were carried out under the same conditions, assigning random initial velocities to each of them, followed by warming to 278 K using a decreasing positional restraint. These simulations were performed on a small cluster of single-processor Pentium

IV (3.0 GHz) computers. For both the LCMD and each of the 8CMD simulations, protein coordinates were saved every 0.2 ps and the initial 25 ns were omitted for analysis, unless otherwise stated.

2.2. Hamiltonian Replica Exchange. For a system composed of N atoms with coordinate vectors and momentum vectors denoted respectively by $\mathbf{q} \equiv \{q_1, \dots, q_N\}$ and $\mathbf{p} \equiv \{p_1, \dots, p_N\}$, the Hamiltonian is the sum of the kinetic energy $K(\mathbf{p})$ and the potential energy $E(\mathbf{q})$:

$$H(\mathbf{q}, \mathbf{p}) = K(\mathbf{p}) + E(\mathbf{q}) \quad (1)$$

Let us now consider one step of a simple H-REMD simulation at constant inverse temperature $\beta = 1/k_B T$ on two replicas i and j , with coordinate vectors \mathbf{q}_i and \mathbf{q}_j and momentum vectors \mathbf{p}_i and \mathbf{p}_j , simulated respectively with the two Hamiltonians H_m and H_n , which differ only in their form of the potential energy:

$$H_k(\mathbf{q}, \mathbf{p}) = K(\mathbf{p}) + E_k(\mathbf{q}) \quad (k = m \text{ or } n) \quad (2)$$

This corresponds to a state Ω in the generalized ensemble

$$\Omega = \{H_m(\mathbf{q}_i, \mathbf{p}_i), H_n(\mathbf{q}_j, \mathbf{p}_j)\} \quad (3)$$

An exchange of Hamiltonians between the two replicas can be described as

$$\Omega = \{H_m(\mathbf{q}_i, \mathbf{p}_i), H_n(\mathbf{q}_j, \mathbf{p}_j)\} \rightarrow \Omega' = \{H_n(\mathbf{q}_i, \mathbf{p}_i), H_m(\mathbf{q}_j, \mathbf{p}_j)\} \quad (4)$$

In order for this exchange process to converge toward an equilibrium distribution, the condition of detailed balance must be imposed on the exchange probability $w(\Omega \rightarrow \Omega')$ ¹⁵, leading to

$$w(\Omega \rightarrow \Omega') \equiv \min[1, \exp(-\Delta)] \quad (5)$$

with

$$\Delta \equiv \beta[E_n(\mathbf{q}_i) - E_m(\mathbf{q}_i) + E_m(\mathbf{q}_j) - E_n(\mathbf{q}_j)] \quad (6)$$

which is independent of the individual momenta of the two replicas.

Writing the potential-energy term of Hamiltonian k as

$$E_k(\mathbf{q}) = V_u(\mathbf{q}) + \sum_{l=1}^L \mu_{l,k} V_l(\mathbf{q}) \quad (7)$$

where $V_u(\mathbf{q})$ incorporates the unmodified part of the function and $\mu_{l,k}$ are the factors by which the $V_l(\mathbf{q})$ terms are scaled; Δ in eq 6 further reduces to

$$\Delta \equiv \beta \sum_{l=1}^L (\mu_{l,n} - \mu_{l,m}) [V_l(\mathbf{q}_i) - V_l(\mathbf{q}_j)] \quad (8)$$

Thus, the exchange probability is only dependent on the modified part of the potential-energy function.

On the basis of the GROMOS 43a1 force-field and combination rules, we generated modified force fields multiplying the charges of side-chain protein atoms and the C6^{1/2} and C12^{1/2} LJ parameters of all protein atoms by a factor $f_k < 1$. The 1–4 LJ parameters, which are defined separately in the GROMOS force fields, were not scaled.

Hence, in our case, L is equal 2, and eq 7 becomes

$$E_k(\mathbf{q}) = V_u(\mathbf{q}) + f_k V_1(\mathbf{q}) + f_k^2 V_2(\mathbf{q}) \quad (9)$$

where V_1 represents the sum of all LJ protein–solvent interactions and electrostatic interactions between side-chain and main-chain atoms as well as between side-chain atoms and the solvent. V_2 accounts for the sum of LJ interactions between protein atoms and electrostatic interactions between side-chain atoms. Charges and LJ parameters of all solvent particles, including ions, were left unchanged. The spacing between factors f was chosen such that they would decrease roughly exponentially, and their exact values were tuned, by means of few short trial simulations, to yield exchange probabilities of roughly 20%. Seven modified force fields were thus generated, with f values of 0.965, 0.931, 0.898, 0.867, 0.837, 0.808, and 0.780. They were used, along with the unmodified GROMOS 43a1 force field, to run a 100 ns H-REMD simulation on eight replicas, starting from the same initial structure as that in the LCMD simulation, and attempting pairwise replica exchanges every 10 ps. Protein coordinates were saved every 50 fs, and the initial 25 ns of the simulation were omitted for analysis, unless otherwise stated. This simulation was run on a cluster consisting of eight dual-processor Pentium III (750 MHz) nodes.

2.3. Weighted Histogram Analysis Method. Data produced during REMD simulations can be combined using the weighted histogram analysis method (WHAM).^{39,40} The algorithm was originally developed for umbrella-sampling simulations but can easily be adapted to our H-REMD approach by reformulating the potential-energy function corresponding to the i th force field in the following way:

$$E_i = E_0 + \lambda_{1,i} V_1 + \lambda_{2,i} V_2 \quad \lambda_{1,i} = f_i - 1; \lambda_{2,i} = f_i^2 - 1 \quad (10)$$

where E_0 is the potential energy computed with the unmodified force field, while the scaling factor f_i and the potentials V_1 and V_2 are like those in eq 9. This form of the potential-energy function corresponds to that used in umbrella-sampling simulations.

Since we performed our H-REMD simulation at a constant temperature, the WHAM equations become independent of the value of E_0 ⁴¹ and can be formulated in terms of the values of the biasing potentials V_1 and V_2 only:

$$\exp(-g_i) = \frac{\sum_{k=1}^R \sum_{t=1}^n \exp(-\beta \lambda_{1,i} V_{1,t}^{(k)} - \beta \lambda_{2,i} V_{2,t}^{(k)})}{\sum_{m=1}^R \sum_{t=1}^n \exp[g_m - \beta \lambda_{1,m} V_{1,t}^{(k)} - \beta \lambda_{2,m} V_{2,t}^{(k)}]} \quad (i = 1, \dots, R) \quad (11)$$

where R is the number of replicas, n the number of snapshots used for the analysis, g_i a dimensionless free energy for the force field i , and $V_{(1,2),t}^{(k)}$ represents the value of the biasing potential for replica k at time t . After iterating the set of equations in eq 11 to self-consistency of the values of g_i , an un-normalized statistical weight P_0 is obtained for each time

point t of each replica k , which has the form

$$P_0(k,t) = \left[\sum_{m=1}^R n \exp(g_m - \beta \lambda_{1,m} V_{1,t}^{(k)} - \beta \lambda_{2,m} V_{2,t}^{(k)}) \right]^{-1} \quad (12)$$

and gives the probability of sampling point t of replica k with the unmodified force field.

2.4. Free-Energy Landscapes. As described in detail by Tavernelli et al.,⁴² a two-dimensional representation of the FEL can be obtained from simulated atomic trajectories by plotting the negative logarithm of the joint probability distribution of two global parameters, ξ_1 and ξ_2 . The resulting graph is a projection of the relative FEL, in units of $k_B T$, on a plane defined by the two global parameters. In the case of H-REMD simulations, the probability distribution must be calculated in a weighted manner; we did this using the WHAM-derived statistical weights.

2.5. Native Contacts. For the definition of a set of native contacts in CRT18, we have used the atomic trajectory between 250 and 750 ps of our LCMD simulation. Each residue was partitioned into main-chain and side-chain atoms, and the minimum interatomic distance between these groups was calculated for all snapshots in the trajectory, taking into account only amino acids at least three residues apart along the polypeptide chain. To be included in the list of native contacts, pairs had to display interatomic distances lower than 0.37 nm for at least 60% of the time. By this procedure, we have identified 25 native contacts, each of which was assigned a weight corresponding to its fractional presence during the 500 ps LCMD simulation segment. Summing up the weights of the resulting matrix, we have obtained a normalization factor F .

The existence of native contacts in all our simulations was monitored and scored by means of the matrix derived as just discussed. For each snapshot along a simulated trajectory, we defined the fraction of native contacts (FNC) as the sum of the weights-matrix elements corresponding to the native contacts present at that time, divided by the normalization factor F . Our analysis also included a monitoring of the total number of contacts as a function of time.

2.6. Clustering. We performed a structural clustering of the simulated ensembles using the algorithm described by Daura et al.⁴³ The procedure is based on the calculation of a matrix of the pairwise positional root-mean-square deviation (RMSD), after least-squares superposition, and the choice of a cutoff to define the neighborhood of each cluster. The structure with the largest number of neighbors is considered to be the center of the largest cluster, and it is removed, together with its neighbors, from the pool of structures before again searching for the next largest cluster. This procedure is repeated until all structures in the ensemble are clustered.

In our clustering analyses, we used a cutoff of 0.1 nm and considered only the backbone atoms of residues 3–16 (see Figure 1), both for the least-squares fitting and for the computation of the RMSD. To give different weights to the structures obtained with modified Hamiltonians during the H-REMD simulation, we did the clustering analysis using structures averaged over 5 ps intervals. For the classical MD

simulations, the weight of a cluster is equal to the number of its members divided by the total number of structures used for the clustering. In the case of the H-REMD simulation, the weight of a cluster equals the sum of the 5-ps-averaged WHAM weights of its members, normalized by the sum of the WHAM weights for the whole ensemble.

2.7. Correlation Coefficients. As a criterion to compare the convergence efficiency of the H-REMD to that of the 8CMD simulation, we have calculated the Pearson's correlation coefficients resting on 1D probability distributions of RMSD and FNC, WHAM-weighted in the case of H-REMD. This was done by computing the correlation coefficient $r(t)$, defined as

$$r(t) = \frac{[\sum_{i=1}^N P_t(i) P_0(i)] - N^{-1} \sum_{i=1}^N P_t(i) \sum_{i=1}^N P_0(i)}{\sqrt{\{[\sum_{i=1}^N P_t^2(i)] - N^{-1} [\sum_{i=1}^N P_t(i)]^2\} \{[\sum_{i=1}^N P_0^2(i)] - N^{-1} [\sum_{i=1}^N P_0(i)]^2\}}} \quad (13)$$

where $P_t(i)$ and $P_0(i)$ refer respectively to the probability distribution for bin i between 25 ns and time t and to that computed between 25 ns and 100 ns. Since the summations of $P_t(i)$ and $P_0(i)$ over all bins are equal to 1, eq 13 reduces to

$$r(t) = \frac{\sum_i P_t(i) P_0(i) - \frac{1}{N}}{\sqrt{\left\{ \left[\sum_{i=1}^N P_t^2(i) \right] - \frac{1}{N} \right\} \left\{ \left[\sum_{i=1}^N P_0^2(i) \right] - \frac{1}{N} \right\}}} \quad (14)$$

2.8. Comparison with NMR Data. To compare our simulations with experimental data, we used a set of upper bounds for the distances between pairs of hydrogen atoms belonging to different amino acids, as derived by nuclear Overhauser effect (NOE) measurements carried out by P. Bettendorff and L. Ellgaard (Institutes of Biochemistry and Molecular Biology and Biophysics, ETH-Zurich, unpublished results). The comparison was based on 126 unambiguous inter-residue interproton distances. These upper bounds were determined assuming the NOE intensity to be inversely proportional to the sixth power of the interproton distance. We therefore compared the simulated ensemble averages $\langle d^{-6} \rangle^{-1/6}$ (using WHAM weighting for the H-REMD simulation) with the upper bounds derived from NMR data.

3. Results and Discussion

The goal of REMD simulations is to enhance conformational space sampling compared to that of classical MD. The basic idea behind T-REMD simulations is to let the system experience elevated temperatures, thereby allowing it to more easily overcome high-energy barriers separating conformational states. Instead, in our H-REMD approach, we use different Hamiltonians with modified nonbonded interaction parameters, to enhance conformational space sampling not only by altering the height of energy barriers but also by

affecting the frustration of the system and, therefore, its dynamic properties.¹⁹ To our knowledge, this is the first report on a H-REMD simulation in an explicit solvent that also deals with a direct comparison to the results of the same number of classical MD simulations of identical length and those of a single, longer one. Previous H-REMD simulations have been carried out, for instance, by Fukunishi et al.¹⁶ and Jang et al.⁴⁴ The former authors compared T-REMD to two variants of H-REMD, one using scaled hydrophobicity and the other phantom chains that allow various degrees of atomic overlaps and, therefore, the polypeptide chain to cross over itself. The simulations were carried out using a "coarse-grained" protein model in which (i) the solvent effect is implicitly accounted for via solvation free energy; (ii) the backbone includes three united atoms per amino acid, that is, NH, CH, and CO; and (iii) the side chains, except for glycine, are simplified as spheres placed at the center of mass of the residue. Using a 16-residue polyalanine and the albumin-binding domain of protein A, Fukunishi et al.¹⁶ show that the scaled hydrophobicity method is most efficient. On the other hand, Jang et al.⁴⁴ used a generalized effective potential to achieve a change in the effective temperature of the system by modifying the torsional and nonbonded terms of the potential energy function. They carried out a 4.1 ns H-REMD simulation at 100 K (referred to as q -REM in their article), on an alanine dipeptide in vacuo, showing that two replicas, with q values of 1 and 1.002, are as good as at least five replicas in T-REMD of the same length, with temperatures of 100, 123, 148, 178, and 213 K.

3.1. H-REMD Protocol and WHAM. We tested several approaches to modify the individual terms describing the nonbonded interactions of a protein in water, namely, reducing only the LJ potentials between protein atoms, lowering exclusively the partial charges of side-chain atoms, or a combination of the two. The last approach (eq 9) gave the best results, both in terms of efficiency in sampling the conformational space and in terms of diffusion of the individual replicas in the space defined by the different Hamiltonians.

Crucial for the success of a replica exchange simulation is that (a) the exchanges occur frequently enough, such that each replica samples the whole range of the different conditions used for the simulation several times, and (b) the time gap between two exchange attempts is longer than the autocorrelation time of the potential energy. For our modified Hamiltonians, the autocorrelation time was determined to be in the sub-picosecond range. Therefore, one can assume a period of 10 ps between exchange attempts to be long enough to ensure quasi-independence of a replica-exchange step from the previous one.

As described in Section 2.2, we carried out short trial simulations to adjust the scaling factors f —used to prepare the modified force fields—to yield replica exchange probabilities of $\sim 20\%$. This is neither a guarantee that the same probability levels are maintained for a longer simulation, where large conformational changes might influence them, nor does it ensure that each replica samples the whole range of simulation conditions. However, the data reported in Table 1 show that the average exchange probabilities between

Table 1. Percentages of Force Field Exchange during the H-REMD Simulation^a

scaling factor	0.965	0.931	0.898	0.867	0.837	0.808	0.780
1.000	18.56	0.26	0.00	0.00	0.00	0.00	0.00
0.965		18.37	0.22	0.00	0.00	0.00	0.00
0.931			19.33	0.53	0.01	0.00	0.00
0.898				20.97	0.49	0.00	0.00
0.867					22.74	0.42	0.00
0.837						21.36	0.63
0.808							25.19

^a Average exchange percentages between the individual force fields used in the H-REMD simulation computed from the entire trajectories. Force fields are represented by the scaling factors f used to modify the electrostatic and LJ parameters (see Section 2.2).

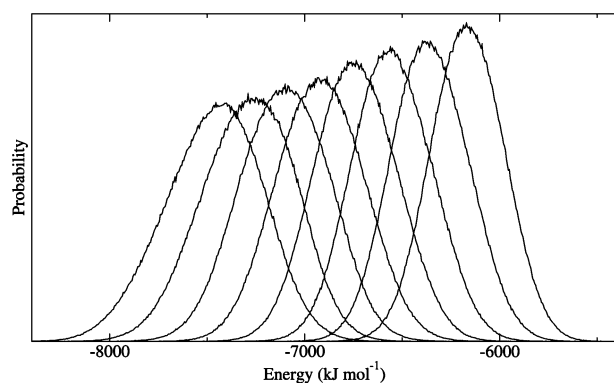


Figure 2. Histograms of the sum of the terms V_1 and V_2 in eq 9 for the individual force fields, as obtained from the whole 100 ns H-REMD simulation. The left-most and right-most curves correspond to the structural ensembles simulated respectively with the unmodified and most strongly modified force fields. The curves for neighboring force fields overlap considerably, ensuring sufficiently large replica-exchange probabilities.

neighboring force fields, when calculated for the whole simulation period of 100 ns, were sufficiently large. Furthermore, Figure 2 shows that neighboring histograms of the sums of the terms V_1 and V_2 in eq 9 display considerable overlap, a prerequisite for frequent replica exchanges. The curves depicted in Figure 2 sample a broad energy range, with the histograms being centered at $-7420 \text{ kJ mol}^{-1}$ and $-6160 \text{ kJ mol}^{-1}$ respectively for the unmodified and the most strongly modified force fields. During the 100 ns simulation, each replica sampled all force fields, although some spent most of their time in only a subset of them (Table 2). To give a more complete picture of the efficiency with which replicas have repeatedly used the different simulation conditions, we report in Figure 3 the force-field trajectories of the two limit cases, namely, those of replicas 2 and 3. Replica 3 sampled the various force fields most evenly, whereas replica 2 showed the most skewed distribution, nevertheless keeping a good sampling efficiency through all force fields. The average time for a replica to move from the unmodified force field to the most strongly modified one was 1770 ps (188 observations), for the reverse process, 1988 ps (184 observations), while a return to the unmodified force field via the most strongly modified one lasted on average 3886 ps (184 observations).

Table 2. Percentage Sampling of the Individual Force Fields by Each Replica during the H-REMD Simulation^a

scaling factor	1.000	0.965	0.931	0.898	0.867	0.837	0.808	0.780
replica 1	19.82	18.25	15.43	12.88	12.07	9.60	6.87	5.08
replica 2	4.86	6.12	8.23	9.67	10.89	13.05	19.72	27.46
replica 3	10.74	12.19	12.98	12.23	13.65	13.34	13.57	11.30
replica 4	7.88	10.35	12.79	14.98	16.25	15.10	12.17	10.48
replica 5	6.60	7.59	9.56	13.58	14.66	15.77	15.95	16.29
replica 6	20.81	17.45	14.15	11.09	9.05	9.15	8.65	9.65
replica 7	6.94	8.65	10.40	12.78	13.75	15.21	16.24	16.03
replica 8	22.35	19.40	16.46	12.79	9.68	8.78	6.83	3.71

^a Percentages refer to the sampling of the individual force fields by each replica for the whole simulation period of 100 ns of the H-REMD simulation. The individual force fields are represented by the scaling factors f used to modify the electrostatic and LJ parameters (see Section 2.2), whereas replicas are numbered arbitrarily.

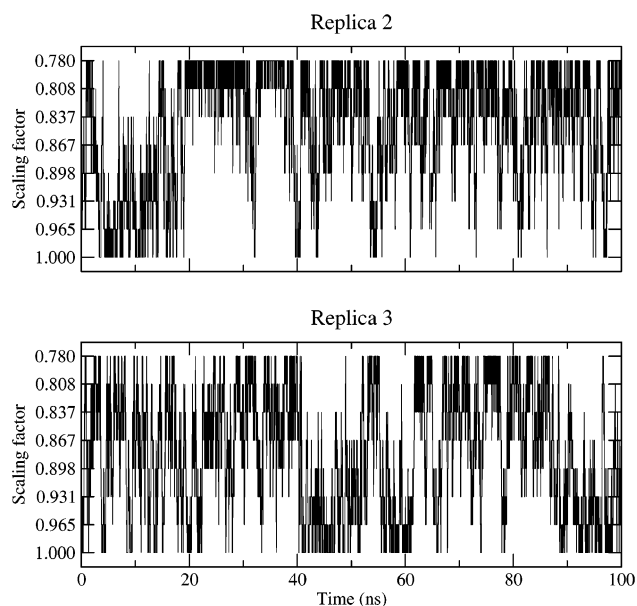


Figure 3. Force-field trajectories of two selected replicas of the H-REMD simulation. Both replicas sample each force field several times. Among all of the replicas, number 2 displays the most skewed and number 3 the most even distribution of the sampled force fields. The individual force fields are indicated on the y axis by the scaling factors f used to modify the nonbonded interaction parameters (see Section 2.2).

To account for the simulations being performed with different force fields, we assigned to each time point of each replica a statistical weight using WHAM (eqs 11 and 12). When normalized by the average weight assigned to the structures generated using the unmodified force field, the coordinates produced with the most strongly modified force field were assigned an average weight of ca. 5×10^{-9} . Thus, the influence on thermodynamic quantities of the data generated with the most strongly modified force fields is on average very small. However, a certain overlap still exists even between the most extreme situations, since the lowest weight assigned to any frame simulated with the unmodified force field is smaller than the highest weight assigned to any frame simulated with the most strongly modified Hamiltonian. So it is not the case that one could simply omit the data produced by the strongly modified force fields.

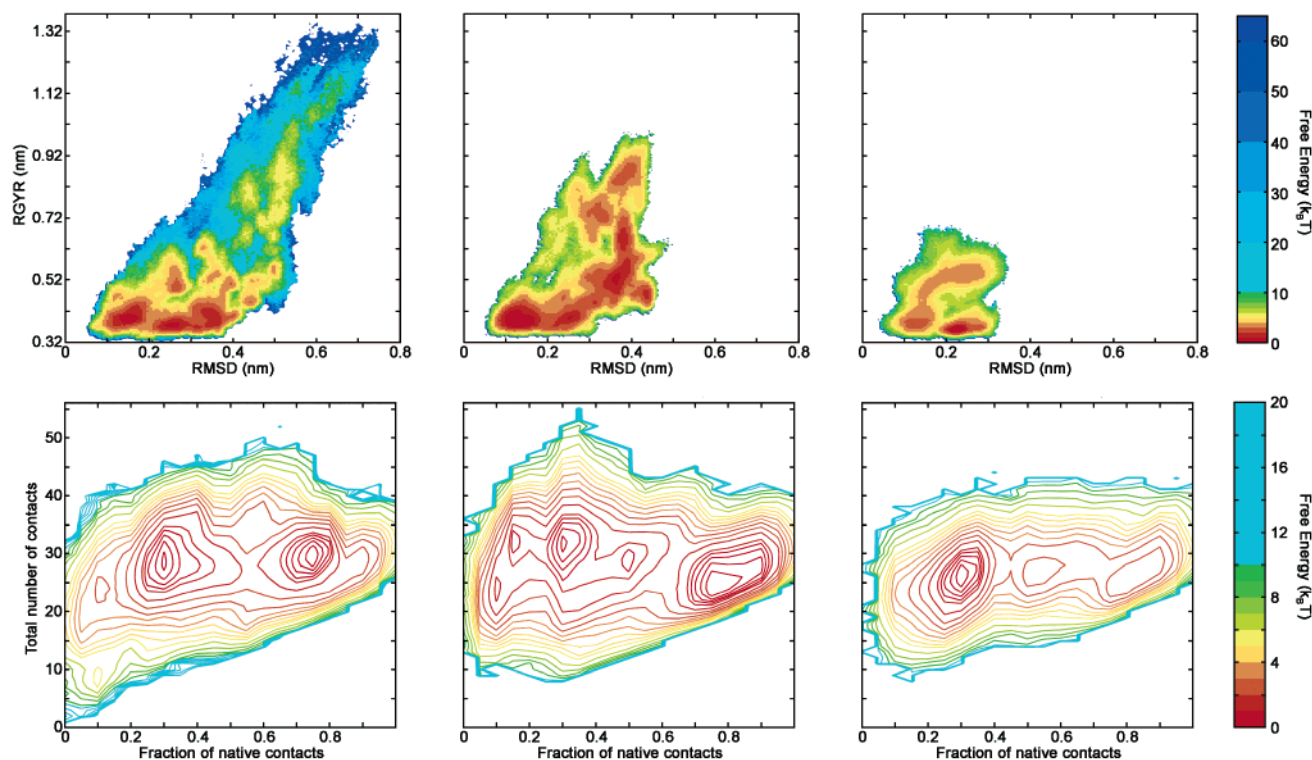


Figure 4. Comparison of two-dimensional representations of the free-energy landscapes for the three simulation approaches we have used. The upper row shows representations resting on the RMSD of the backbone atoms of residues 3–16 from the reference structure and the radius of gyration of the hydrophobic-core atoms (for structural details, see Figure 1). The lower row shows the projection of the free-energy landscapes on the plane defined by the FNC and the total number of contacts. The first column refers to the WHAM-weighted results of the H-REMD simulation, the second column to those of the 8CMD simulation, and the third to those of the LCMD simulation. The first 25 ns of each simulation were omitted from the analysis. Contour lines are drawn every $0.2 k_B T$ between 0 and $1 k_B T$, every $0.5 k_B T$ in the interval $1-5 k_B T$, every $1 k_B T$ between 5 and $10 k_B T$, and every $2 k_B T$ in the interval $10-20 k_B T$. All graphs are normalized to a minimum of $0 k_B T$. Figures were generated with MATLAB 6.5.

3.2. Free-Energy Landscapes. Enhanced sampling of the conformational space entails avoiding a trapping of the system within local energy minima through repeated exchanges of the simulation conditions among replicas. Therefore, a way to judge the efficiency in conformational space sampling is the comparison of two-dimensional representations of the FEL computed from structural ensembles simulated with different methods. After having tested several global parameters for the FEL representations, we have selected those that most clearly describe the situation, namely, the backbone RMSD of residues 3–16 relative to our reference structure (for details, see Figure 1), the radius of gyration of the hydrophobic core (RGYR), the FNC, and the total number of contacts. The FEL representations thus obtained from our three simulation approaches are depicted in Figure 4. By far, the LCMD simulation samples the smallest region of the conformational space (third column of Figure 4). For the 8CMD simulations, the volume of the visited conformational space is considerably increased (middle column in Figure 4), but with our H-REMD approach, we were able to increase it even further. The states sampled during the H-REMD simulation reach RGYR values 3.5-fold higher than that of the reference structure, equal to 0.374 nm , and a RMSD greater than 0.7 nm , compared respectively to a 2.8-fold-increased RGYR and a largest RMSD value of $\sim 0.5 \text{ nm}$ observed in the 8CMD simulation.

A careful comparison of the two left-most FEL representations in the top row of Figure 4 reveals that minima characterized by increasing RGYR and RMSD values are less well-defined in the H-REMD compared to the 8CMD simulation. We can envisage several plausible explanations for this phenomenon. The first is intrinsically related to the REMD approach, which does not allow the system to extensively explore energy minima. Furthermore, low probability states, likely to be characterized by high values of RGYR and RMSD, are given full weight in the computation of the FEL for the 8CMD simulations, but not so in the case of the H-REMD simulation due to WHAM weighting. Finally, as discussed in Section 3.3, neither simulation approach has reached structural convergence; therefore, the corresponding FEL representations cannot be expected to match completely.

From the FELs shown in Figure 4, it appears that CRT18 frequently visits two states during the simulations, one quite close to the reference structure and the other clearly different, although still characterized by a compact hydrophobic core, but with a small FNC. For a computation of relative free energies to be statistically relevant, it is necessary that a system repeatedly move back and forth between individual states. A projection of the trajectories onto the two-dimensional FELs representations offers a simple way to test if this condition is satisfied. For instance, in the FELs presented in the second row of Figure 4, we can define the

region characterized by a FNC below 0.3 as unfolded, and above 0.75 as folded, and thereafter analyze how often the system moves back and forth among the two regions. Using snapshots taken at 0.2 ps intervals, we observe a total of 30 folding and 32 unfolding events in the H-REMD simulation between 25 and 100 ns, compared to 7 and 12 in the 8CMD, or 6 and 7 during the 25–450 ns LCMD simulation period, none of which occurring in the first 100 ns. The choice of other boundaries for the definition of folded and unfolded regions does not significantly influence the results. For example, defining the boundaries at FNC values of 0.35 and 0.7 yields 102 folding and 105 unfolding events in the H-REMD simulation, compared to 51 and 55 in the 8CMD, or 27 and 28 for the period 25–450 ns of the LCMD simulation, again none of which occurring in the first 100 ns. These results prove that transitions between individual free-energy minima occur more easily in the H-REMD simulation than in either of the CMD ones, thus, implying a better definition of the minima in the FEL representations corresponding to the H-REMD (left column of Figure 4) compared to the ones in the 8CMD (central column) and LCMD (right column) simulations.

In our simulations, the FNC ranges from 1 to 0. The complete sampling of this structural parameter allows us to analyze the percentage of formation of single contacts as a function of the FNC, with the aim of identifying contacts possibly involved in early folding events. For this purpose, we partitioned the FNC into evenly spaced bins, and each snapshot of the simulated ensembles was assigned to the bin corresponding to its FNC. For each bin, we then calculated the fraction of times any given contact was present (data not shown). Although one cannot expect to identify true folding paths from a REMD simulation, the results of this analysis indicate that folding of CRT18 might be facilitated by the formation of contacts between residues 8 and 12, at the tip of the hairpin, as well as between tryptophans 7 and 15.

3.3 Clustering. As an alternative means to quantify conformational space sampling, one can perform a structural clustering and compare both the total number of clusters obtained from the entire coordinates ensemble and how the number of clusters changes as a function of time. We carried out a structural clustering based on a matrix of pairwise RMSDs, following the algorithm described in Section 2.6, which guarantees the distance between cluster centers to be not smaller than the chosen cutoff value. Generally, using snapshots of simulations taken every 10 ps is considered sufficient, since large conformational changes are not expected to occur on this time scale.⁴³ Instead of taking snapshots, we have used, for our analyses, coordinate averages over 5 ps such that, when dealing with REMD simulation data, cluster weights could be computed from the WHAM weights of their members. Figure 5 shows the results of this analysis for the H-REMD and the 8CMD simulations. Using a cutoff of 0.1 nm for the RMSD between the backbone atoms of residues 3–16, we identified 798 clusters in the H-REMD simulation and only 273 in the 8CMD simulations. Comparing the number of clusters with a weight larger than a certain threshold (panels B–D in Figure 5)

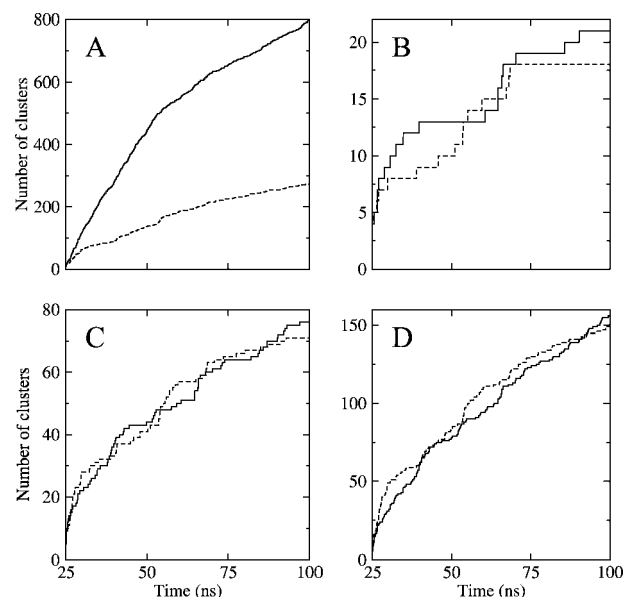


Figure 5. Number of clusters sampled as a function of time during the H-REMD (solid lines) and the 8CMD (dashed lines) simulations, as computed from the whole ensemble of conformations produced by each simulation. Panel A refers to the time courses of the total number of clusters, panel B to those of clusters with weights greater than 1% of all conformations considered, panel C to the ones with weights larger than 0.1%, and panel D to clusters whose weight exceeds 0.01%. The analysis has been done on coordinate averages over 5 ps to allow, in the case of H-REMD, a weighting of the clusters based on the WHAM weights of their members. For additional details, see Section 2.6.

reveals that this difference mainly stems from poorly populated clusters with weights below 0.01%. The final slopes of the curves depicted in Figure 5 show that, with neither simulation approach, clustering has reached convergence. However, comparing the time courses of the total number of clusters and those with weights greater than 1%, namely, neglecting structures simulated with strongly modified force fields, further confirms the improvement in conformational space sampling obtained with our H-REMD approach compared to 8CMD. For instance, after 40 ns, 13 clusters with final weights greater than 1% are already defined in the H-REMD data set, compared to 9 in the 8CMD simulations. To analyze the H-REMD simulation, we also tested a clustering algorithm slightly different from the one described in the Methods and Analysis section, in which we defined the center of a cluster to be the structure whose neighbors have the largest sum of WHAM weights, rather than that with the largest number of neighbors. The two algorithms produce comparable results, the structures of the largest cluster centers being very similar, as well as the cluster sizes (data not shown). The only notable differences are the total number of clusters (822 as compared to 798) and an increase in the number of clusters formed by only a few members. On the basis of these findings, we decided to use the clustering algorithm described in Section 2.6, also because it can be applied to both the H-REMD and the 8CMD simulations, thus allowing a direct comparison of the results.

Figure 5 shows that the H-REMD and the 8CMD simulations display a comparable time evolution of the number of clusters with weights greater than 0.1% (panel C) and 0.01% (panel D). Since there is an apparently large overlap between the FEL representations computed from the H-REMD and those that stem from the 8CMD simulations (Figure 4), one could argue that the two simulations sample the same region of the conformational space and that the H-REMD approach simply extends the conformational sampling toward unfolded structures. However, comparing the conformations corresponding to the centers of the 20 most populated clusters reveals that many of those occurring in one simulation are not sampled by the other. This difference can easily be rationalized considering that our representations of the FEL are highly degenerate. Hence, basins that appear to be well-defined actually result from the superposition of numerous minima, which cannot be distinguished by the collective entities used to reduce a hyperdimensional space to two dimensions. This explains the apparent large overlap between the two-dimensional FEL representations computed from the H-REMD and the 8CMD simulations, despite the relative dissimilarity between the 20 most populated cluster centers. Still, as can be seen in Figure 6, the structures corresponding to the center of the largest cluster of the H-REMD (structure B) and 8CMD (structure C) simulations are almost identical (backbone RMSD of 0.076 nm, heavy-atoms RMSD of 0.168 nm) and, if one neglects the N- and C-terminal residues, highly similar to the reference structure. Furthermore, the largest clusters are of comparable size in the two simulations, being populated by 15.68% and 18.60% respectively for the H-REMD and 8CMD approaches. A totally different situation applies to the LCMD simulation, where the most populated cluster (structure D in Figure 6) is clearly different from the reference structure.

Figure 6 further illustrates the improved efficiency of our H-REMD protocol, compared to 8CMD and LCMD, in sampling the conformational space. The configurations corresponding to the center of the cluster with the largest RMSD from the reference structure are still quite compact in the 8CMD and LCMD simulations (respectively structures F and G in Figure 6), whereas that relative to the H-REMD simulation with an unmodified force field (structure E in Figure 6) is almost fully extended. A visual inspection of the atomic trajectories of the single replicas in the H-REMD simulation reveals that, during the simulation, CRT18 completely unfolded—and refolded to a compact state—in several replicas.

3.4. Correlation Coefficients. The results discussed so far consistently show that our H-REMD protocol is more efficient in sampling the conformational space compared to classical simulation approaches. The clustering analysis just discussed also provides some information in this respect. As another independent approach to compare the simulation protocols used in our investigation, we have computed with eq 14 the correlation coefficients depicted in Figure 7. We used 100 bins of sizes 0.01 nm and 0.01 respectively for RMSD (left panel) and FNC (right panel), whereas t was incrementally increased by 100 ps, starting from 25 ns up to 100 ns, leading to 750 P distributions. The time courses

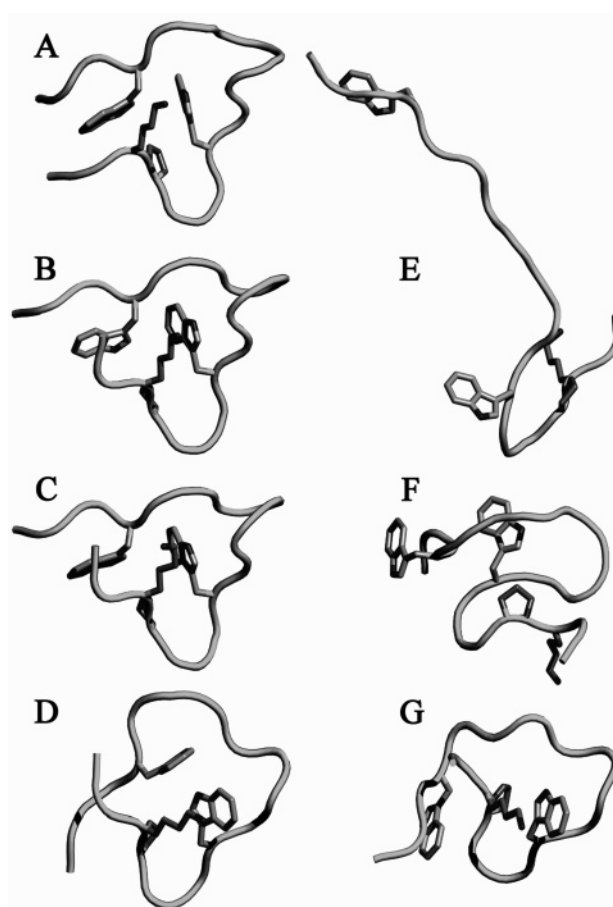


Figure 6. Models of the reference structure of CRT18 (A), of the conformations corresponding to the centers of the most populated clusters (B for H-REMD, C for 8CMD, and D for LCMD), and of the centers of the clusters with the largest RMSD from structure A (E for H-REMD with $f = 1$, F for 8CMD, and G for LCMD). Structures averaged over 5 ps intervals were used for the clustering, excluding the initial 25 ns of each simulation, which resulted in a total of 1.2×10^5 structures for both the H-REMD and the 8CMD simulations and 8.5×10^4 structures for the LCMD simulation. The backbone/all-atoms RMSD from A, for residues 3–16, are 0.1045/0.2042 nm for B, 0.0983/0.2234 nm for C, and 0.2240/0.4276 nm for D. The models were drawn using PYMOL (<http://www.pymol.org>).

of the correlation coefficient for both parameters show that the H-REMD simulation (continuous curves) converges more rapidly compared to the 8CMD (dashed traces) simulation, the difference being particularly pronounced for the FNC.

3.5. Comparison with NMR Data. During a simulation, one not only wishes to sample as large a volume of the conformational space as possible but also reproduce structural features measured experimentally. We have, therefore, compared our simulated ensembles with the upper bounds of inter-residue interproton distances d derived from NOE measurements at 278 K. The whole set of 126 unambiguous interproton distances identified from NMR data (see Section 2.8) has been used for the comparison. The graphs in the top-left, top-right, and bottom-left panels of Figure 8 show the ensemble averages $\langle d^{-6} \rangle^{-1/6}$, computed respectively from the 8CMD, H-REMD, and LCMD simulations, plotted

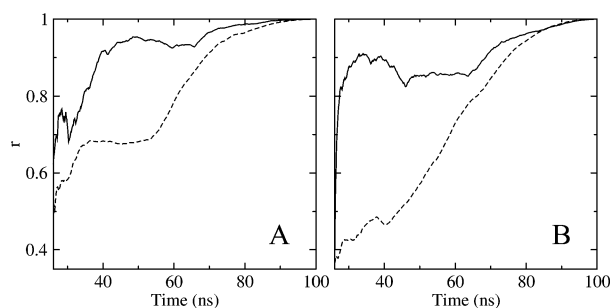


Figure 7. Time series of the correlation coefficients computed with eq 14 for the RMSD of the backbone atoms of residues 3–16, relative to the reference structure (left panel), and for the FNC (right panel). The solid lines refer to WHAM-weighted H-REMD data, whereas the dashed curves correspond to the 8CMD simulations. More details are given in Section 2.7.

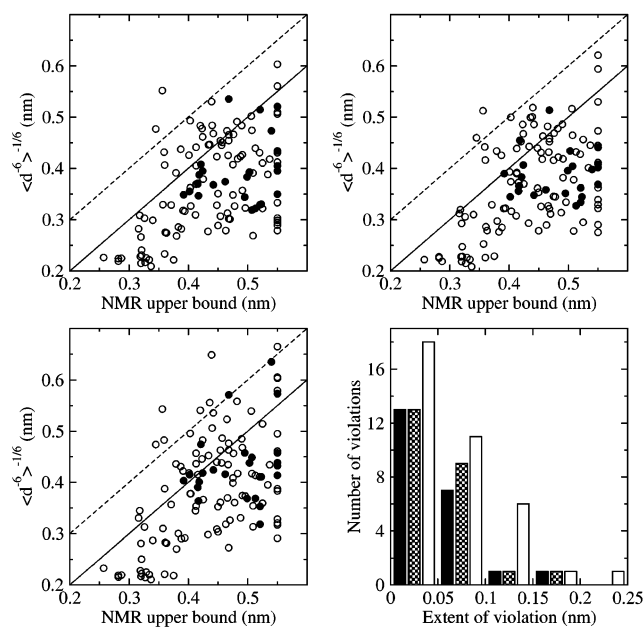


Figure 8. Simulated ensemble averages of interproton distances $\langle d^{-6} \rangle^{-1/6}$, plotted against upper bounds of the same distances derived from NOE measurements. A set of 126 unambiguous interproton distances was used for the analysis (see Section 2.8). The upper-left panel refers to the simulation 8CMD, the upper-right to the H-REMD, and the lower left to the LCMD. In all three cases, filled circles represent distances between protons belonging to amino acids at least four residues apart along the polypeptide chain. The solid diagonal lines indicate the boundary above which the experimental distances are violated, whereas the dashed lines represent the boundary above which such distances are violated by more than 0.1 nm. In the lower-right panel, the number of violations is plotted against their extent, with full, dashed, and empty bars referring respectively to the 8CMD, H-REMD, and LCMD simulations. In the case of the H-REMD data, ensemble averages were calculated using WHAM weights.

against the upper bounds of the same interproton distances derived from NMR data. Distinction is made for distances involving amino acids at least four residues apart along the polypeptide chain (filled circles) because they are most indicative of the global structure of the molecule. To give

Table 3. Violated Distances between Individual Pairs of Hydrogen Atoms^a

atoms involved		violations (nm)	
atom 1/residue	atom 2/residue	H-REMD	8CMD
HB2/PRO-4	HN/ASP-6	0.056	0.046
HB2/PRO-4	HN/TRP-7	0.156	0.196
HB2/PRO-4	HB1/TRP-7	0.114	0.131
HB2/PRO-4	HE3/TRP-7	0.032	0.063
HG2/PRO-4	HN/TRP-7	0.070	0.053
HG2/PRO-4	HB1/TRP-7	0.063	0.054
HG2/PRO-4	HE3/TRP-7	0.083	0.072
HD1/TRP-7	HB2/GLU-9	0.061	0.091
HZ2/TRP-7	HB1/ASP-12	0.045	0.067
HB1/ASP-8	HB2/MET-11	0.055	0.021
HB1/ASP-8	HG1/MET-11	0.078	0.044
HB1/MET-11	HA/ASP-12	0.096	0.090
HE1/TRP-15	HD1/PRO-18	0.063	0.010

^a The list includes all hydrogen pairs involved in interproton inter-residue distances violated by more than 0.05 nm with respect to the NMR data in either the H-REMD or the 8CMD simulation.

an overview of the situation, the bottom-right panel of Figure 8 displays the number of violations relative to four distance ranges. The LCMD simulation displays the largest number of violations, in total 37. Instead, despite the diversity of their conformational ensembles, the violations for the H-REMD and 8CMD simulations are comparably few (24 for the former and 22 for the latter), also if only the structures simulated with the unmodified force field are included in the analysis (data not shown). The situation does not change if one considers only the most significant violations, namely, those greater than 0.05 nm (19 for LCMD, 11 for H-REMD, and 9 for 8CMD). Combining the sets of such interproton distance violations occurring in either the H-REMD or 8CMD simulations yields a list of 13 proton pairs, of which 9 involve TRP-7, as shown in Table 3. Clearly, the strongest violations observed in the two approaches involve hydrogen pairs belonging to PRO-4 and TRP-7.

While discussing the time evolution of the FNC, we have postulated the formation of contacts between residues 8 and 12 and between tryptophans 7 and 15 to be early events during folding (next-to-last paragraph of the subsection on free-energy landscapes). Interestingly, the comparison of the simulated ensembles with NMR data shows that the four unequivocal interproton, inter-residue distances involving tryptophans 7 and 15 are never violated during the LCMD and 8CMD simulations, and only one of them, namely, Trp7(HZ2)–Trp15(HA), is moderately violated (by 0.011 nm) exclusively in the LCMD simulation. Furthermore, in all three structural ensembles, the only Asp8–Asp12 unequivocal distance derived from NMR data (HB1–HN) is again never violated.

We have analyzed the ensemble averages $\langle d^{-6} \rangle^{-1/6}$ separately for the individual clusters (data not shown) and found that each of them violates more of the NMR-derived interproton distances, and more severely than if the ensemble average is taken for the whole simulation. This applies even to the most populated cluster, which is very similar to the reference structure. None of the found clusters fits the experimental data better than the whole ensemble of simu-

lated structures. This finding is in agreement with previous reports⁴⁵ indicating that ensemble averages more accurately reproduced NMR data than single structures.

4. Conclusions

Judging from the simulations on the CRT18 fragment reported here, our novel H-REMD approach considerably enhances conformational space sampling compared to classical MD, without affecting the computational effort. The better sampling also involves structures with very small Boltzmann weights, which, however, can potentially have important biological functions. No direct comparison with previous reports on H-REMD simulations on biological macromolecules can be done because the simulation conditions are too different, as described at the beginning of the Results and Discussion section. Compared to T-REMD, our approach allows a fine-tuning of the different simulation conditions used for REMD to specifically influence those degrees of freedom that are of greatest interest, or that are believed to most strongly affect the dynamic properties of the system being investigated. This allows a substantial reduction in the number of replicas needed to perform a REMD simulation, while still permitting an efficient conformational searching. Our results show that the data produced by all the different force fields used for a H-REMD simulation can be successfully combined with WHAM. Furthermore, simulating with modified force fields does not introduce structural artifacts, as demonstrated by the comparison with NMR data and with classical simulation approaches. The results reported here support our premise that acting on the frustration of nonbonded interactions influences conformational-space sampling. Last, but not least, our simulations favor the hypothesis that, contrary to what has been observed for longer fragments of the calreticulin P domain, CRT18 does not fold to a unique structure.

Acknowledgment. This work was supported by the ETH Zurich with Grants 0-20915-01 and 0-50590-04. The authors thank Pascal Bettendorff and Lars Ellgaard for kindly providing NMR data on CRT18 prior to their publication and Daniele Passerone, Lars Ellgaard, and Xavier Daura for stimulating discussions. The constructive criticisms and suggestions by the reviewers of this article are also kindly acknowledged.

References

- (1) Balabin, L. A.; Onuchic, J. N. Dynamically Controlled Protein Tunneling Paths in Photosynthetic Reaction Centers. *Science* **2000**, *290*, 114–117.
- (2) Mitsutake, A.; Sugita, Y.; Okamoto, Y. Generalized-ensemble algorithms for molecular simulations of biopolymers. *Biopolymers* **2001**, *60* (2), 96–123.
- (3) Berg, B. A.; Neuhaus, T. Multicanonical algorithms for first-order phase transitions. *Phys. Lett.* **1991**, *267* (2), 249–53.
- (4) Berg, B. A.; Neuhaus, T. Multicanonical ensemble: A new approach to simulate first-order phase transitions. *Phys. Rev. Lett.* **1992**, *68* (1), 9–12.
- (5) Lyubartsev, A. P.; Martinovski, A. A.; Shevkunov, S. V.; Vorontsov-Velyaminov, P. N. New approach to Monte Carlo calculations of the free energy: Method of expanded ensembles. *J. Chem. Phys.* **1992**, *96* (3), 1776–83.
- (6) Marinari, E.; Parisi, G. Simulated tempering: A new Monte Carlo scheme. *Europhys. Lett.* **1992**, *19*, 451–58.
- (7) Sugita, Y.; Okamoto, Y. Replica-exchange molecular dynamics method for protein folding. *Chem. Phys. Lett.* **1999**, *314*, 141–51.
- (8) Sugita, Y.; Okamoto, Y. Replica-exchange multicanonical algorithm and multicanonical replica-exchange method for simulating systems with rough energy landscape. *Chem. Phys. Lett.* **2000**, *329*, 261–70.
- (9) Sugita, Y.; Kitao, A.; Okamoto, Y. Multidimensional replica-exchange method for free-energy calculations. *J. Chem. Phys.* **2000**, *113* (15), 6042–51.
- (10) Yamamoto, R.; Kob, W. Replica-exchange molecular dynamics simulation for supercooled liquids. *Phys. Rev. E: Stat. Phys., Plasmas, Fluids, Relat. Interdiscip. Top.* **2000**, *61* (5B), 5473–6.
- (11) Okabe, T.; Kawata, M.; Okamoto, Y.; Mikami, M. Replica-exchange Monte Carlo method for the isobaric–isothermal ensemble. *Chem. Phys. Lett.* **2001**, *335*, 435–9.
- (12) Sanbonmatsu, K. Y.; Garcia, A. E. Structure of Met-enkephalin in explicit aqueous solution using replica exchange molecular dynamics. *Proteins* **2002**, *46* (2), 225–34.
- (13) Hukushima, K. Domain-wall free energy of spin-glass models: numerical model and boundary conditions. *Phys. Rev. E: Stat., Nonlinear, Soft Matter Phys.* **1999**, *60* (4), 3606–3614.
- (14) Gront, D.; Kolinski, A.; Skolnick, J. Comparison of three Monte Carlo conformational search strategies for a protein-like homopolymer model: Folding thermodynamics and identification of low-energy structures. *J. Chem. Phys.* **2000**, *113* (12), 5065–71.
- (15) Hukushima, K.; Nemoto, K. Exchange Monte Carlo method and application to spin glass simulations. *J. Phys. Soc. Jpn.* **1996**, *65* (4), 1604–8.
- (16) Fukunishi, H.; Watanabe, O.; Takada, S. On the Hamiltonian replica exchange method for efficient sampling of biomolecular systems: Application to protein structure prediction. *J. Chem. Phys.* **2002**, *116* (20), 9058–67.
- (17) Murata, K.; Sugita, Y.; Okamoto, Y. Molecular dynamics simulations of DNA dimers based on replica-exchange umbrella sampling II: Free energy analysis. *J. Theor. Comput. Chem.* **2005**, *4*, 433–448.
- (18) Snow, C. D.; Sorin, E. J.; Rhee, Y. M.; Pande, V. How well can simulation predict protein folding kinetics and thermodynamics. *Annu. Rev. Biophys. Biomol. Struct.* **2005**, *34*, 43.
- (19) Tavernelli, I.; Di Iorio, E. E. The interplay between protein dynamics and frustration of nonbonded interactions as revealed by molecular dynamics simulations. *Chem. Phys. Lett.* **2001**, *345*, 287–294.
- (20) Wolynes, P. G.; Eaton, W. A. The physics of protein folding. *Phys. World* **1999**, *12*, 39–44.
- (21) Bryngelson, J. D.; Onuchic, J. N.; Socci, N. D.; Wolynes, P. G. Funnels, pathways, and the energy landscape of protein folding: A synthesis. *Proteins* **1995**, *21* (3), 167–95.
- (22) Piela, L.; Kostrowicki, J.; Scheraga, H. A. The multiple-minima problem in the conformational analysis of molecules. Deformation of the potential energy hypersurface by the diffusion equation method. *J. Chem. Phys.* **1989**, *93*, 3339–3346.

- (23) Kostrowicki, J.; Scheraga, H. A. Application of the diffusion equation method for global optimization to oligopeptides. *J. Chem. Phys.* **1992**, *96*, 7442–7449.
- (24) Schug, A.; Herges, T.; Wenzel, W. Reproducible protein folding with the stochastic tunneling method. *Phys. Rev. Lett.* **2003**, *91* (15), 158102.
- (25) Pappu, R. V.; Marshall, G. R.; Ponder, J. W. A potential smoothing algorithm accurately predicts transmembrane helix packing. *Nat. Struct. Mol. Biol.* **1999**, *6* (1), 50–55.
- (26) Ellgaard, L.; Frickel, E.-M. Calnexin, calreticulin and ERp57: teammates in glycoprotein folding. *Cell Biochem. Biophys.* **2003**, *39*, 223–248.
- (27) Ellgaard, L.; Bettendorff, P.; Braun, D.; Herrmann, T.; Fiorito, F.; Jelesarov, I.; Guntert, P.; Helenius, A.; Wuthrich, K. NMR structures of 36 and 73-residue fragments of the calreticulin P-domain. *J. Mol. Biol.* **2002**, *322* (4), 773–84.
- (28) Ellgaard, L.; Riek, R.; Braun, D.; Herrmann, T.; Helenius, A.; Wuthrich, K. Three-dimensional structure topology of the calreticulin P-domain based on NMR assignment. *FEBS Lett.* **2001**, *488* (1–2), 69–73.
- (29) Ellgaard, L.; Riek, R.; Herrmann, T.; Guntert, P.; Braun, D.; Helenius, A.; Wuthrich, K. NMR structure of the calreticulin P-domain. *Proc. Natl. Acad. Sci. U.S.A.* **2001**, *98* (6), 3133–8.
- (30) Berendsen, H. J. C.; van der Spoel, D.; van Drunen, R. GROMACS: A message-passing parallel molecular dynamics implementation. *Comput. Phys. Commun.* **1995**, *91*, 43–56.
- (31) Lindahl, E.; Hess, B.; van der Spoel, D. GROMACS 3.0: A package for molecular simulation and trajectory analysis. *J. Mol. Model.* **2001**, *7*, 306–17.
- (32) van Gunsteren, W. F.; Billeter, S. R.; Eising, A. A.; Hünenberger, P. H.; Krüger, P.; Mark, A. E.; Scott, W. R. P.; Tironi, I. G. *Biomolecular simulation: The GROMOS96 manual and user guide*; vdf Hochschulverlag AG an der ETH Zurich, BIOMOS b.v. Zurich Groningen: Zurich, Switzerland; Groningen, Netherlands, 1996.
- (33) Berendsen, H. J. C.; Postma, J. P. M.; van Gunsteren, W. F.; Di Nola, A.; Haak, J. R. Molecular dynamics with coupling to an external bath. *J. Chem. Phys.* **1984**, *81*, 3684–3690.
- (34) Hess, B.; Bekker, H.; Berendsen, H. J. C.; Fraaije, J. G. E. M. LINCS: A linear constraint colver for molecular simulations. *J. Comput. Chem.* **1997**, *18*, 1463–72.
- (35) Miyamoto, S.; Kollman, P. A. SETTLE: An analytical version of the SHAKE and RATTLE algorithms for rigid water models. *J. Comput. Chem.* **1992**, *13*, 952–62.
- (36) Tironi, I. G.; Sperb, R.; Smith, P. E.; van Gunsteren, W. F. A generalized reaction field method for molecular dynamics simulations. *J. Chem. Phys.* **1995**, *102*, 5451–5459.
- (37) Smith, P. E.; van Gunsteren, W. F. Consistent dielectric properties of the simple point charge and extended simple point charge water models at 277 and 300 K. *J. Chem. Phys.* **1994**, *100* (4), 3169–74.
- (38) Berendsen, H. J. C.; Grigera, J. R.; Straatsma, T. P. The missing term in effective pair potentials. *J. Chem. Phys.* **1987**, *91* (24), 6269–71.
- (39) Kumar, S.; Bouzida, D.; Swendsen, R. H.; Kollman, P. A.; Rosenberg, J. M. The weighted histogram analysis method for free-energy calculations on biomolecules. I. The method. *J. Comput. Chem.* **1992**, *13* (8), 1011–21.
- (40) Kumar, S.; Rosenberg, J. M.; Bouzida, D.; Swendsen, R. H.; Kollman, P. A. Multidimensional free-energy calculations using the weighted histogram analysis method. *J. Comput. Chem.* **1995**, *16* (11), 1339–50.
- (41) Boczek, E. M.; Brooks, C. L., III. Constant-temperature free energy surfaces for physical and chemical processes. *J. Phys. Chem.* **1993**, *97* (17), 4509–13.
- (42) Tavernelli, I.; Cotesta, S.; Di Iorio, E. E. Protein dynamics, thermal stability, and free-energy landscapes: a molecular dynamics investigation. *Biophys. J.* **2003**, *85* (4), 2641–9.
- (43) Daura, X.; Gademann, K.; Jaun, B.; Seebach, D.; van Gunsteren, W. F.; Mark, A. E. Peptide folding: When simulation meets experiment. *Angew. Chem., Int. Ed.* **1999**, *38*, 236–40.
- (44) Jang, S.; Shin, S.; Pak, Y. Replica-exchange method using the generalized effective potential. *Phys. Rev. Lett.* **2003**, *91* (5), 058305.
- (45) Daura, X.; Gademann, K.; Schafer, H.; Jaun, B.; Seebach, D.; van Gunsteren, W. F. The beta-peptide hairpin in solution: conformational study of a beta-hexapeptide in methanol by NMR spectroscopy and MD simulation. *J. Am. Chem. Soc.* **2001**, *123* (10), 2393–404.
- (46) Kabsch, W.; Sander, C. Dictionary of secondary structure: Pattern recognition of hydrogen-bonded and geometrical features. *Biopolymers* **1983**, *22*, 2577–2637.

CT050250B